Mechanics of Materials 41 (2009) 364–374

Contents lists available at ScienceDirect

Mechanics of Materials

journal homepage: www.elsevier.com/locate/mechmat

Microstructure evolution in hyperelastic laminates and implications for overall behavior and macroscopic stability

O. Lopez-Pamies [a,*], P. Ponte Castañeda [b]

[a] Department of Mechanical Engineering, State University of New York, 139 Light Engineering, Stony Brook, NY 11794-2300, USA
[b] Department of Mechanical Engineering and Applied Mechanics, University of Pennsylvania, Philadelphia, PA 19104-6315, USA

ARTICLE INFO

Article history:
Received 23 July 2008

ABSTRACT

In this paper we study the evolution of the underlying microstructure in hyperelastic laminates subjected to finite deformations. To this end, we identify a set of relevant microstructural variables and derive rigorous formulae for their evolution along finite-deformation paths. Making use of these results we then establish connections between the evolution of the microstructure and the overall stress–strain relation and macroscopic stability in hyperelastic laminates. In particular, we show that the *rotation of the layers* may lead to a reduction in the overall stiffness of the laminates under appropriate loading conditions. Furthermore, we show that this *geometric mechanism* is intimately related to the possible loss of strong ellipticity of the overall behavior of these materials, which may occur even in the case when the underlying constituents are taken to be strongly elliptic.

Published by Elsevier Ltd.

1. Introduction

It is by now well recognized that the effective properties and stability of composites subjected to finite deformations depend strongly on the underlying evolution of microstructure. However, because of the technical difficulties associated with material and geometric nonlinearities proper of finite deformations, the characterization of this phenomenon remains to date largely unresolved. In this regard, the main purpose of this paper is to provide rigorous results characterizing the effect of the evolution of microstructure on the overall properties and stability of a special class of composites for which *exact* analytical solutions may be computed. As an example of such a case, we study in this work the problem of *hyperelastic laminates subjected to finite deformations*.

It is relevant to emphasize here that laminates correspond to limiting microstructures within the broader class of "particulate" microstructures. Thus, the *exact* results to be developed in this work are expected to be useful for guiding the identification and understanding of physical mechanisms inherent in material systems with more general "particulate" morphologies (such as particle- and fiber-reinforced elastomers) for which exact solutions are not accessible in general. In addition, laminate (nano) structures have been observed to appear in a special class of block copolymers of increasing commercial interest, the so-called thermoplastic elastomers (see, e.g., Cohen et al., 2000). The results of this work may thus be utilized to shed some light on the complex mechanical behavior of these materials as well.

2. Problem setting

Consider a two-phase[1] laminate with an alternating layer morphology (see Fig. 1). Such a material is assumed to occupy a volume Ω_0, with boundary $\partial\Omega_0$, in the undeformed configuration. The initial direction of lamination and repeat length are denoted by the unit vector $\mathbf{N}$ and the scalar L_0, respectively (see Fig. 1). Moreover, the initial thicknesses of the layers, denoted by $L_0^{(r)}(r=1,2)$, are

* Corresponding author. Tel.: +1 631 632 8249; fax: +1 631 632 8544.
E-mail addresses: oscar.lopez-pamies@sunysb.edu (O. Lopez-Pamies), ponte@seas.upenn.edu (P. Ponte Castañeda).

[1] The development that follows can be easily generalized to any number of phases.

0167-6636/$ - see front matter Published by Elsevier Ltd.
doi:10.1016/j.mechmat.2009.01.006

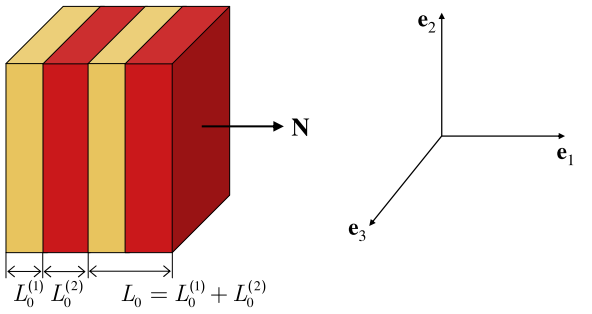

Fig. 1. Schematic (of two repeat lengths) of a hyperelastic laminate in the undeformed configuration. The initial lamination direction and repeat length are given by **N** and L_0, respectively. Note that – for convenience – **N** has been aligned with the laboratory basis vector $\mathbf{e}_1$.

assumed to be *much smaller* than the size of the specimen and the scale of variation of the applied loading.

Material points in the solid are identified by their initial position vector $\mathbf{X}$ in the undeformed configuration Ω_0, while the current position vector of the same point in the deformed configuration Ω is given by $\mathbf{x}$. The deformation gradient $\mathbf{F}$ at $\mathbf{X}$, a quantity that measures the deformation in the neighborhood of $\mathbf{X}$, is defined by:

$$\mathbf{F} = \frac{\partial \mathbf{x}}{\partial \mathbf{X}}, \quad J = \det \mathbf{F} > 0 \quad \text{on} \quad \Omega_0. \tag{1}$$

The constitutive behaviors of the phases, which occupy the subdomains $\Omega_0^{(r)}$ in the undeformed configuration, are characterized by hyperelastic potentials $W^{(r)}$ that are *objective*, *non-convex* functions of the deformation gradient tensor $\mathbf{F}$. Thus, the local stored-energy function of this two-phase system may be conveniently written as follows:

$$W(\mathbf{X}, \mathbf{F}) = \sum_{r=1}^{2} \chi_0^{(r)}(\mathbf{X}) W^{(r)}(\mathbf{F}), \tag{2}$$

where the characteristic functions $\chi_0^{(r)}$, which serve to describe the distribution of the two phases in the undeformed configuration, are equal to 1 if the position vector $\mathbf{X}$ is inside phase r (i.e., $\mathbf{X} \in \Omega_0^{(r)}$) and zero otherwise. More specifically, by exploiting the assumed periodicity of the microstructure:

$$\chi_0^{(r)}(X_1, X_2, X_3) = \chi_0^{(r)}(X_1 + z_1 L_0, X_2 + r_2, X_3 + r_3), \tag{3}$$

where z_1 is an arbitrary integer, r_2 and r_3 are arbitrary real numbers, and the direction of lamination $\mathbf{N}$ has been tacitly identified (without loss of generality) with the laboratory basis vector $\mathbf{e}_1$ (see Fig. 1). The local or microscopic constitutive relation is given by:

$$\mathbf{S} = \frac{\partial W}{\partial \mathbf{F}}(\mathbf{X}, \mathbf{F}), \tag{4}$$

where $\mathbf{S}$ denotes the first Piola-Kirchhoff stress tensor, and sufficient smoothness has been assumed for W on $\mathbf{F}$.

Following (Hill, 1972), the global or macroscopic constitutive relation for the laminate is then given by:

$$\overline{\mathbf{S}} = \frac{\partial \widetilde{W}}{\partial \overline{\mathbf{F}}}, \tag{5}$$

where $\overline{\mathbf{S}} = \langle \mathbf{S} \rangle, \overline{\mathbf{F}} = \langle \mathbf{F} \rangle$ are the *average stress* and *average deformation gradient*, respectively, and

$$\widetilde{W}(\overline{\mathbf{F}}) = \min_{\mathbf{F} \in \mathcal{K}(\overline{\mathbf{F}})} \langle W(\mathbf{X}, \mathbf{F}) \rangle = \min_{\mathbf{F} \in \mathcal{K}(\overline{\mathbf{F}})} \sum_{r=1}^{2} c_0^{(r)} \langle W^{(r)}(\mathbf{F}) \rangle^{(r)} \tag{6}$$

is the *effective stored-energy function*. In the above expressions, the brackets $\langle \cdot \rangle$ and $\langle \cdot \rangle^{(r)}$ denote volume averages – in the undeformed configuration – over the specimen (Ω_0) and over phase r ($\Omega_0^{(r)}$), respectively, so that the scalars $c_0^{(r)} = \langle \chi_0^{(r)} \rangle = L_0^{(r)}/L_0 (r = 1, 2)$ represent the initial volume fractions of the given phases. Furthermore, $\mathcal{K}$ denotes the set of kinematically admissible deformation gradients:

$$\mathcal{K}(\overline{\mathbf{F}}) = \{\mathbf{F} | \exists \mathbf{x} = \mathbf{x}(\mathbf{X}) \quad \text{with} \quad \mathbf{F} = \partial \mathbf{x}/\partial \mathbf{X} \text{ in } \Omega_0, \\ \mathbf{x} = \overline{\mathbf{F}}\mathbf{X} \text{ on } \partial\Omega_0\}. \tag{7}$$

A solution (assuming that it exists) of the Euler–Lagrange Equations associated with the variational problem (6) can be readily computed by assuming constant fields in the different layers and solving for the corresponding (traction and displacement) jump conditions – as is done in the context of linear elasticity (see, e.g., Chapter 9 in the monograph by Milton, 2002). However, because of the non-convexity of W on $\mathbf{F}$, this "principal" solution may bifurcate into different energy solutions at sufficiently large deformations. This point corresponds to the onset of an *instability*, beyond which the applicability of the "principal" solution may become questionable. Following the work of Triantafyllidis and collaborators (see, e.g., Triantafyllidis and Maker, 1985; Geymonat et al., 1993; Triantafyllidis et al., 2006), it is useful to make the distinction between "microscopic" instabilities, that is, instabilities with wavelengths that are small compared to the size of the specimen, and "macroscopic" instabilities, that is, instabilities with wavelengths comparable to the size of the specimen. The computation of "microscopic" instabilities is in general a very difficult task, though, for the class of hyperelastic laminates of interest in this work, "microscopic" instabilities may be computed elegantly by making use of Floquet theory (see, e.g., Triantafyllidis and Maker, 1985 and Nestorvic and Triantafyllidis, 2004). On the other hand, the computation of "macroscopic" instabilities is a much simpler task, since it reduces to the detection of loss of strong ellipticity of the effective stored-energy function of the material evaluated at the above-described "principal" solution (Geymonat et al., 1993). To put this information in a more rigorous setting, we define:

$$\widehat{W}(\overline{\mathbf{F}}) = \operatorname*{stat}_{\mathbf{F} \in \mathcal{K}(\overline{\mathbf{F}})} \sum_{r=1}^{2} c_0^{(r)} \langle W^{(r)}(\mathbf{F}) \rangle^{(r)} \tag{8}$$

as the effective stored-energy function of the laminate evaluated at the "principal" solution (i.e., with piecewise-constant fields). Accordingly, "macroscopic" instabilities may develop in the material whenever the inequality

$$\widehat{K}_{ik} b_i b_k = \widehat{\mathcal{L}}_{ijkl} b_i A_j b_k A_l > 0, \tag{9}$$

ceases[2] to hold true for some $\overline{\mathbf{F}}$ and $\mathbf{b} \otimes \mathbf{A} \neq \mathbf{0}$. In this last expression, $\widehat{K}_{ik} = \widehat{\mathcal{L}}_{ijkl} A_j A_l$ is the effective acoustic tensor

[2] Here and subsequently, Latin indices range from 1 to 3 and the usual summation convention is employed.

and $\widehat{\mathcal{L}} = \partial^2 \widehat{W}(\overline{\mathbf{F}})/\partial \overline{\mathbf{F}}^2$ is the effective incremental elastic modulus characterizing the overall incremental response of the material. By definition, it is plain that $\widetilde{W}(\overline{\mathbf{F}}) = \widehat{W}(\overline{\mathbf{F}})$ from $\overline{\mathbf{F}} = \mathbf{I}$ up to the onset of the *first* instability, after which $\widetilde{W}(\overline{\mathbf{F}}) \leqslant \widehat{W}(\overline{\mathbf{F}})$. Incidentally, for the class of laminates of interest in this work, it is often the case (Triantafyllidis and Maker, 1985; Nestorvic and Triantafyllidis, 2004) that the first instability is of infinite wavelength,[3] and hence $\widetilde{W}(\overline{\mathbf{F}}) = \widehat{W}(\overline{\mathbf{F}})$ all the way up to the development of a macroscopic instability, as characterized by the violation of condition (9).

The main concern of this paper is the study of the stationary variational problem (8). In particular, we are interested in determining from the solution of (8) not only the overall constitutive behavior of hyperelastic laminates (up to the onset of "macroscopic" instabilities), but also the associated evolution of microstructure in these materials. In this regard, it should be emphasized that – because of the Lagrangian description of the kinematics – the solution of (8) contains implicitly all the necessary information to describe how every point in the specimen moves, and therefore, also how the microstructure evolves. Ultimately, the objective of this work is to explore the effect of the evolution of microstructure on the overall response, as well as on the development of "macroscopic" instabilities in the class of hyperelastic laminates defined above.

3. Effective properties of hyperelastic laminates

As already stated, the solution to the variational problem (8) can be constructed by assuming constant fields per phase and solving for the appropriate (traction and displacement) jump conditions. In this work, however, we follow a different route and make use of the tangent second-order homogenization method (Ponte Castañeda and Tiberio, 2000) to solve (8). The alternative use of this method proves helpful to gain further insight on the effective behavior of hyperelastic laminates. To avoid loss of continuity here, the pertinent derivations are given in Appendices A and B. Next, we summarize the final expressions that characterize the overall constitutive response and microstructure evolution in hyperelastic laminates.

3.1. Overall constitutive behavior

In order to spell out the relevant expressions that describe the effective constitutive behavior of hyperelastic laminates, it proves helpful to define (for clarity of notation) the unit vectors $\mathbf{N}^{\perp 2} \doteq \mathbf{e}_2$ and $\mathbf{N}^{\perp 3} \doteq \mathbf{e}_3$, such that $\mathbf{N}^{\perp 2} \cdot \mathbf{N} = \mathbf{N}^{\perp 3} \cdot \mathbf{N} = \mathbf{N}^{\perp 2} \cdot \mathbf{N}^{\perp 3} = 0$, where it is recalled that the initial direction of lamination $\mathbf{N} = \mathbf{e}_1$ (see Fig. 1). It then follows that the *effective stored-energy function* (8) for the above-defined class of laminates, made up of two phases characterized by the stored-energy functions $W^{(1)}$ and $W^{(2)}$ with corresponding initial volume fractions $c_0^{(1)}$ and $c_0^{(2)}$, may be written as (see Appendix A for details):

$$\widehat{W}(\overline{\mathbf{F}}) = c_0^{(1)} W^{(1)}(\overline{\mathbf{F}}^{(1)}) + c_0^{(2)} W^{(2)}(\overline{\mathbf{F}}^{(2)}). \tag{10}$$

[3] This is indeed the case when the stiffer layers are sufficiently thick.

Here, the average deformation gradient in phase 2, $\overline{\mathbf{F}}^{(2)} = \langle \mathbf{F} \rangle^{(2)}$, is given explicitly by the global average condition

$$\overline{\mathbf{F}}^{(2)} = \frac{1}{c_0^{(2)}} \overline{\mathbf{F}} - \frac{c_0^{(1)}}{c_0^{(2)}} \overline{\mathbf{F}}^{(1)}, \tag{11}$$

while the average deformation gradient in phase 1, $\overline{\mathbf{F}}^{(1)} = \langle \mathbf{F} \rangle^{(1)}$, must be determined from relations

$$[\overline{\mathbf{F}} - \overline{\mathbf{F}}^{(1)}]\mathbf{N}^{\perp 2} = \mathbf{0}, [\overline{\mathbf{F}} - \overline{\mathbf{F}}^{(1)}]\mathbf{N}^{\perp 3} = \mathbf{0}, \tag{12}$$

and

$$[\boldsymbol{\mathcal{S}}^{(1)}(\overline{\mathbf{F}}^{(1)}) - \boldsymbol{\mathcal{S}}^{(2)}(\overline{\mathbf{F}}^{(2)})]\mathbf{N} = \mathbf{0}, \tag{13}$$

where the notation $\boldsymbol{\mathcal{S}}^{(r)}(\cdot) = \partial W^{(r)}(\cdot)/\partial \mathbf{F}$ has been introduced for convenience. Note that conditions (12) correspond to nothing more than the jump conditions across the layer interfaces required to ensure continuity of the deformation vector field in the hyperelastic composite. Similarly, condition (13) is nothing more than the jump condition across the layer interfaces required to ensure static equilibrium. From a computational point of view, it is also interesting to note that relations (12) constitute a system of 6 *linear*, algebraic equations for 6 components of $\overline{\mathbf{F}}^{(1)}$. Solving these equations renders:

$$\overline{\mathbf{F}}^{(1)} = \overline{\mathbf{F}} + \mathbf{a} \otimes \mathbf{N}, \tag{14}$$

where $\mathbf{a}$ is an arbitrary vector (with 3 unknown components). On the other hand, relation (13) constitutes a system of 3 *nonlinear*, algebraic equations for the remaining 3 components of $\overline{\mathbf{F}}^{(1)}$. In general, this last system of 3 equations must be solved numerically, but depending on the functional character of $W^{(1)}$ and $W^{(2)}$, possible simplifications may be carried out.

The *average* (or *macroscopic*) *stress* and *effective incremental modulus tensor* associated with the effective stored-energy function (10) may be conveniently written as follows (see Appendix A for details):

$$\overline{\mathbf{S}} = \frac{\partial \widehat{W}}{\partial \overline{\mathbf{F}}}(\overline{\mathbf{F}}) = c_0^{(1)} \boldsymbol{\mathcal{S}}^{(1)}(\overline{\mathbf{F}}^{(1)}) + c_0^{(2)} \boldsymbol{\mathcal{S}}^{(2)}(\overline{\mathbf{F}}^{(2)}) \tag{15}$$

and

$$\widehat{\mathcal{L}} = \frac{\partial^2 \widehat{W}}{\partial \overline{\mathbf{F}}^2}(\overline{\mathbf{F}}) = \boldsymbol{\mathcal{L}}^{(1)}(\overline{\mathbf{F}}^{(1)}) + c_0^{(2)}[c_0^{(1)}\mathbf{H} - (\boldsymbol{\mathcal{L}}^{(1)}(\overline{\mathbf{F}}^{(1)}) - \boldsymbol{\mathcal{L}}^{(2)}(\overline{\mathbf{F}}^{(2)}))^{-1}]^{-1}, \tag{16}$$

respectively. In this last relation, $\boldsymbol{\mathcal{L}}^{(r)}(\cdot) = \partial^2 W^{(r)}(\cdot)/\partial \mathbf{F}^2$ and

$$H_{ijkl} = K_{ik}^{-1} N_j N_l, \tag{17}$$

where $K_{ik} = \mathcal{L}^{(1)}_{ipkq}(\overline{\mathbf{F}}^{(1)}) N_p N_q$ and it is recalled that the unit vector $\mathbf{N}$ denotes the direction of lamination in the undeformed configuration, as depicted by Fig. 1. Note that – similar to the effective stored – energy function (10) – expressions (15) and (16) depend solely on $\overline{\mathbf{F}}^{(1)}$ and $\overline{\mathbf{F}}^{(2)}$, and *not* on their derivatives with respect to the macroscopic deformation gradient $\overline{\mathbf{F}}$ (e.g., $\partial \overline{\mathbf{F}}^{(1)}/\partial \overline{\mathbf{F}}$).

3.2. Microstructure evolution

The preceding expressions provide rigorous results that completely characterize the mechanical response of hyperelastic laminates subjected to finite deformations. In this subsection, with the aim of gaining a more fundamental understanding on the effective behavior of these materials, we identify a set of relevant microstructural variables and provide rigorous explicit expressions for their evolution along a given macroscopic loading path (see Appendix B for the relevant derivations).

The relevant microstructural variables are identified here as (see Lopez-Pamies (2006) for a generalization of these notions to other systems): (i) the current volume fraction of the constituents, $c^{(1)}$ and $c^{(2)}$, (ii) the current lamination direction, $\mathbf{n}$, and (iii) the current repeat length of the laminate, L, in the deformed configuration (see Fig. 2).

The *volume fractions* of the phases in the deformed configuration can be shown to be given by:

$$c^{(1)} = \frac{\det \overline{\mathbf{F}}^{(1)}}{\det \overline{\mathbf{F}}} c_0^{(1)} \quad \text{and} \quad c^{(2)} = \frac{\det \overline{\mathbf{F}}^{(2)}}{\det \overline{\mathbf{F}}} c_0^{(2)}. \tag{18}$$

On the other hand, the current *direction of lamination* can be expediently expressed as:

$$\mathbf{n} = \|\overline{\mathbf{F}}^{-T}\mathbf{N}\|^{-1}\overline{\mathbf{F}}^{-T}\mathbf{N}. \tag{19}$$

Finally, the initial *repeat length* of the laminate L_0 can be shown to evolve to:

$$L = \|\overline{\mathbf{F}}^{-T}\mathbf{N}\|^{-1} L_0 \tag{20}$$

in the deformed configuration.

In connection with the above relations, it is important to make the following two remarks. First, as explained in full detail in Appendix B, it should be emphasized that the derivation of expressions (18)–(20) relies critically on the fact that the exact (i.e., before the development of instabilities) deformation gradient tensor is constant per phase (i.e., $\mathbf{F}(\mathbf{X}) = \overline{\mathbf{F}}^{(r)}$ for $\mathbf{X} \in \Omega_0^{(r)}$). Second, expression (19) for the lamination direction $\mathbf{n}$, as well as relation (20) for the repeat length L, depend on the initial microstructure – via $\mathbf{N}$ and L_0 – and the macroscopic deformation gradient $\overline{\mathbf{F}}$, but *not* on the constitutive behavior of the phases. By contrast, expressions (18) for the current volume fractions $c^{(1)}$ and $c^{(2)}$ *do* depend on the constitutive behavior of the phases through the deformation averages $\overline{\mathbf{F}}^{(1)}$ and $\overline{\mathbf{F}}^{(2)}$ (as determined by Eqs. (11)–(13)).

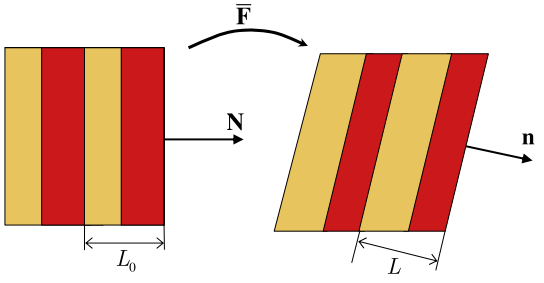

Fig. 2. Schematic representation of the evolution of the direction of lamination and the repeat length along a loading path with macroscopic deformation gradient $\overline{\mathbf{F}}$.

4. A representative example

The results presented in the previous section apply to general hyperelastic potentials, $W^{(1)}$ and $W^{(2)}$, and general loading conditions, $\overline{\mathbf{F}}$. In this section, attention is restricted to specific stored-energy functions for the phases, as well as to specific loading conditions, in an attempt to illustrate – in a transparent manner – the overall properties of hyperelastic laminates subjected to finite deformations. Of special interest is to establish the effect of the microstructure evolution on the overall response and macroscopic stability of these materials.

Thus, attention is restricted to compressible Neo-Hookean stored-energy functions of the form

$$W^{(1)}(\mathbf{F}) = \frac{\mu^{(1)}}{2}(\mathbf{F}\cdot\mathbf{F} - 3) - \mu^{(1)}\ln(\det\mathbf{F}) + \left(\frac{\kappa^{(1)}}{2} - \frac{\mu^{(1)}}{3}\right)(\det\mathbf{F} - 1)^2 \tag{21}$$

and

$$W^{(2)}(\mathbf{F}) = tW^{(1)}(\mathbf{F}), \tag{22}$$

where the material parameters $\mu^{(1)}$ and $\kappa^{(1)}$ denote, respectively, the shear and bulk moduli of phase 1 at zero strain, and the scalar t quantifies the heterogeneity contrast between the layers. Furthermore, attention is restricted to isochoric, plane-strain deformations of the form

$$\overline{F}_{ij} = \begin{bmatrix} \cos\overline{\theta} & -\sin\overline{\theta} & 0 \\ \sin\overline{\theta} & \cos\overline{\theta} & 0 \\ 0 & 0 & 1 \end{bmatrix} \begin{bmatrix} \overline{\lambda} & 0 & 0 \\ 0 & \overline{\lambda}^{-1} & 0 \\ 0 & 0 & 1 \end{bmatrix} \begin{bmatrix} \cos\overline{\theta} & \sin\overline{\theta} & 0 \\ -\sin\overline{\theta} & \cos\overline{\theta} & 0 \\ 0 & 0 & 1 \end{bmatrix}, \tag{23}$$

where (see Fig. 3) $\overline{\lambda} \geqslant 1$ and $\overline{\lambda}^{-1}$ denote the in-plane principal stretches associated with $\overline{\mathbf{F}}$, while $\overline{\theta} \in [0, \pi/2]$ characterizes the orientation (in the counterclockwise sense relative to the fixed laboratory frame of reference) of the in-plane Lagrangian principal axes (i.e., the principal axes of $\overline{\mathbf{F}}^T\overline{\mathbf{F}}$).

The restriction (23) to macroscopic plane-strain deformations has the direct implication that the current direction of lamination $\mathbf{n}$, as determined by expression (19), remains in the $\mathbf{e}_1 - \mathbf{e}_2$-plane. In this connection, it proves expedient for later use to introduce the scalar variable ϕ as the angle – measured in the counterclockwise sense – that characterizes (see Fig. 3) the relative orientation of $\mathbf{n}$ with respect to the lamination direction in the undeformed configuration $\mathbf{N}$. Thus, making use of (19) and (23): $\mathbf{n} = (\cos\phi, \sin\phi, 0)^T$ with

$$\phi = \cos^{-1}\left[\frac{\sqrt{2}(\cos^2\overline{\theta} + \overline{\lambda}^2\sin^2\overline{\theta})}{\sqrt{1 + \overline{\lambda}^4 - (\overline{\lambda}^4 - 1)\cos 2\overline{\theta}}}\right]. \tag{24}$$

4.1. Results and discussion

In the sequel, results are provided for the effective constitutive response, macroscopic stability, and micro-

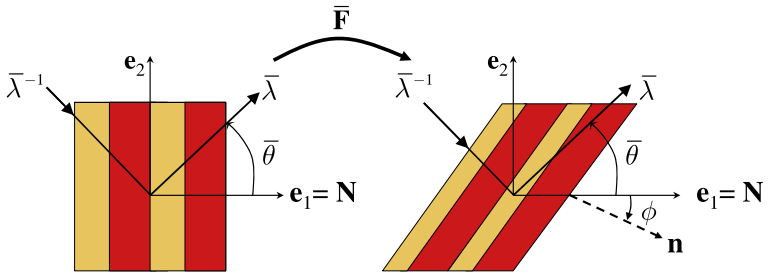

Fig. 3. Pictorial representation of the applied loading conditions, as determined by relation (23), and the angle ϕ determined by (24).

structure evolution in hyperelastic laminates with compressible Neo-Hookean phases characterized by stored-energy functions (21) and (22), subjected to a wide range of loading conditions of the form (23). Results are given for $\mu^{(1)} = 1$, $\kappa^{(1)} = 100$, various values of heterogeneity contrast t, and initial volume fraction $c_0^{(2)} = c_0$. For clarity, the points at which loss of strong ellipticity is first encountered (i.e., the points at which condition (9) is first violated) are denoted with the symbol "$\circ$" in the plots.

4.1.1. Effective constitutive response

Figs. 4 and 5 deal with the effective response and microstructure evolution in Neo-Hookean laminates subjected to pure shear loading (23) at the fixed angles $\overline{\theta} = 0^\circ, 20^\circ, 40^\circ, 45^\circ, 50^\circ, 70^\circ$, and 90°. The results shown in these figures are for contrast $t = 20$ and initial volume fraction $c_0 = 30\%$, and are presented as functions of the macroscopic stretch $\overline{\lambda}$. Parts (a) of the figures show the macroscopic stress $\mathrm{d}\widehat{W}/\mathrm{d}\overline{\lambda}$, while parts (b) depict the corresponding angle of rotation of the layers ϕ (in degrees).

Fig. 4 emphasizes the *large*-deformation regime, while Fig. 5 emphasizes the *small*-deformation regime. We begin by noting that Fig. 5 is consistent with the well-known linearized response of laminated materials. Thus, for infinitesimal deformations, the $\overline{\theta} = 45^\circ$ orientation, which essentially corresponds to simple shear along the layers, provides the softest response (smallest modulus), while the $\overline{\theta} = 0$ and 90° orientations yield the stiffest responses. More generally, as can be seen from Fig. 5a, loadings at complementary angles lead to identical effective responses for small deformations (to order $(\overline{\lambda} - 1)$), in accordance with the linear theory. As the deformation progresses into the finite-deformation regime, the overall stress–stretch relations at complementary angles deviate from each other, with the stiffest response being attained at the largest of the two angles. To understand this difference in the macroscopic response of the laminate, we turn to Fig. 5b, where it is seen that the rotations of the layers for loadings at complementary angles are also initially identical (up to order $(\overline{\lambda} - 1)$) but then deviate slightly. In fact, because of this reorientation of the microstructure (recall that the loading axes are fixed), the laminate is being loaded at continuously varying orientations as the deformation progresses. Now, comparing for example the $\overline{\theta} = 20^\circ$ and 70° initial orientations, it is noted that, as the deformation progresses, the $\overline{\theta} = 20^\circ$ initial orientation becomes more favorably oriented to the softer "shear-along-the-layers" mode, while on the contrary, the 70° initial orientation becomes less favorably oriented to the softer mode of deformation. This is the reason why the $\overline{\theta} = 20^\circ$ initial orientation becomes more compliant than the 70° initial

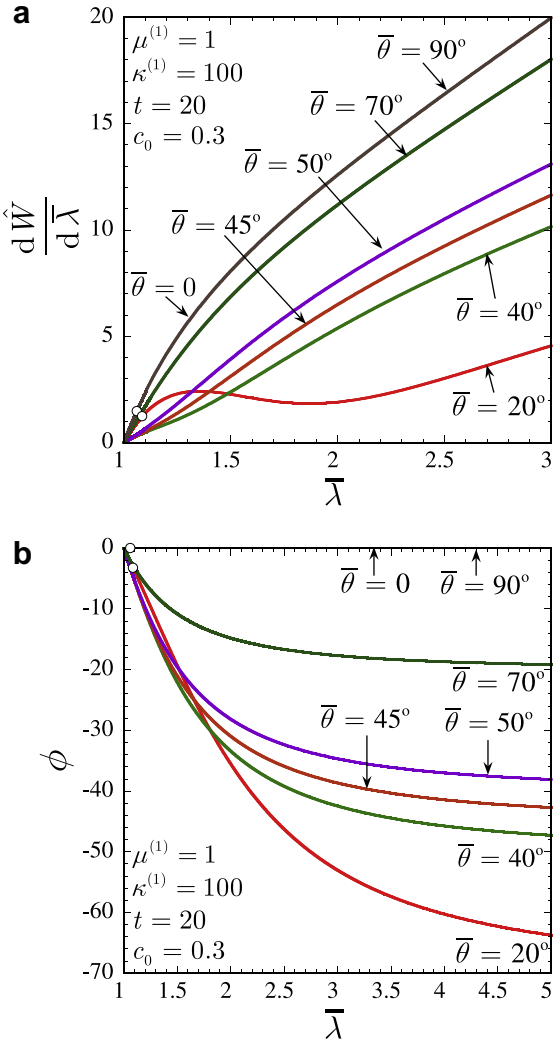

Fig. 4. Effective behavior and microstructure evolution in a hyperelastic laminate subjected to pure shear loading at various angles $\overline{\theta}$. The results correspond to compressible Neo-Hookean phases with contrast $t = 20$, initial volume fraction of the stiffer phase $c_0 = 30\%$, and are shown as a function of the macroscopic stretch $\overline{\lambda}$. (a) The macroscopic stress $\mathrm{d}\widehat{W}/\mathrm{d}\overline{\lambda}$. (b) The angle of rotation of layers ϕ.

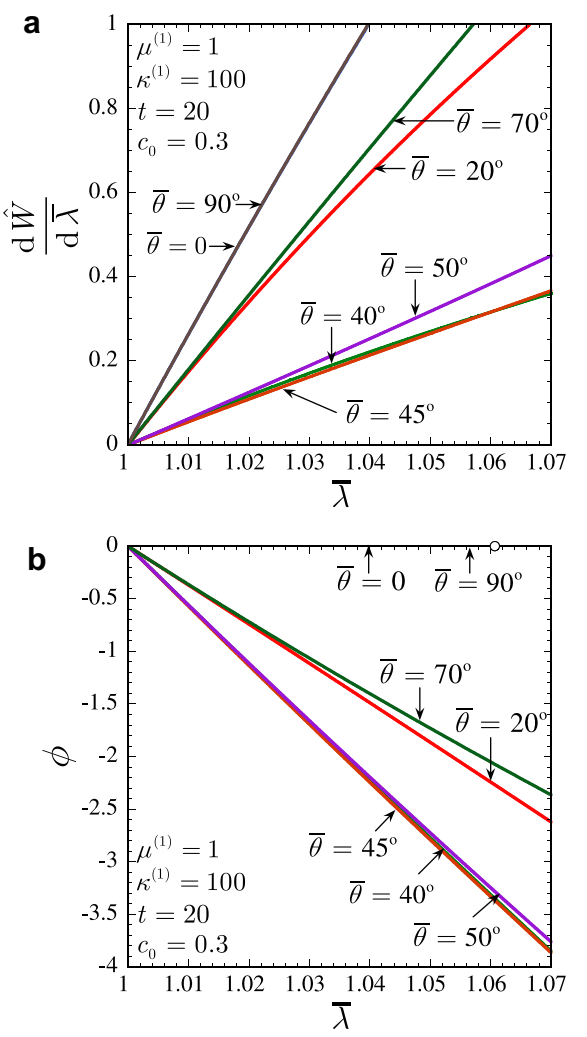

Fig. 5. Effective behavior and microstructure evolution in a hyperelastic laminate subjected to pure shear loading at various angles $\overline{\theta}$ (in the *small*-deformation regime). The results correspond to compressible Neo-Hookean phases with contrast $t = 20$, initial volume fraction of the stiffer phase $c_0 = 30\%$, and are shown as a function of the macroscopic stretch $\overline{\lambda}$. (a) The macroscopic stress $d\widehat{W}/d\overline{\lambda}$. (b) The angle of rotation of layers ϕ.

orientation, as the deformation progresses. Similarly, the $\overline{\theta} = 40^\circ$ initial orientation becomes more compliant than the 50°. On the other hand, the $\overline{\theta} = 0^\circ$ and 90° initial orientation remain essentially identical beyond $O(\overline{\lambda} - 1)$ because in these two highly symmetric cases, there is no reorientation of the microstructure. Therefore, in summary, the reorientation of the layers can lead to either stiffening or to softening (in the sense of making the response less compliant) depending on whether such reorientation tends to make the laminate more or less favorably oriented for the stiffer deformation modes.

Focusing next on Fig. 4a, it is observed that the large-deformation behavior of the laminate is quite different from the small-deformation behavior shown in Fig. 5a. Indeed, for large deformations, the weakest response is associated with the smallest values of the initial orientation angle $\overline{\theta} > 0$. This is once again seen to be a consequence of the reorientation of the layers, depicted in Fig. 4b, which is largest for the smallest values of $\overline{\theta} > 0$ and tends to position the laminate in the most compliant direction (towards 45°).

For example, for $\overline{\theta} = 20^\circ$, the layers are initially oriented at 70° relative to the loading axes, and according to Fig. 4b, the layers reach the softest orientation of 45° relative to the loading axis, when the macroscopic stretch $\overline{\lambda}$ reaches a level of about 1.7, which as can be seen in Fig. 4a corresponds approximately to the low point of the valley in the stress–stretch relation. After this point, the layers keep rotating, but their orientation becomes progressively less favorable to easy shear, and the overall stress–stretch curve is seen to start increasing again. For $\overline{\theta} = 40^\circ$, a similar effect is observed, but at much smaller stretches, since the layers reach the most favorable orientation for shear-along-the-layers at a much smaller overall stretch. For angles $\overline{\theta}$ greater than 45°, there is no initial softening and the overall stress–stretch curves only exhibit a slight stiffening effect, which is in agreement with the fact that the layers become more and more susceptible to the stiff mode of deformation corresponding to axial stretch along the layers. Finally, it should be emphasized in the context of Fig. 4 that the case of $\overline{\theta} = 0$ is an exception since the perfect alignment of the layers with the loading suppresses the rotation. In fact, the initial response of the $\overline{\theta} = 0$ case, though slightly more compliant, is essentially identical to that at $\overline{\theta} = 90^\circ$. However, although the reorientation of the layers is suppressed for this "principal" $\overline{\theta} = 0$ solution, the tendency to relieve stress through rotation is still there and eventually leads to a macroscopic instability, characterized by loss of ellipticity and denoted in the plots with the symbol "∘". A similar phenomenon takes place for the case of $\overline{\theta} = 20^\circ$, even though the laminate is able to accommodate some stress through rotation of the microstructure in this case. For the other, larger angles depicted ($\overline{\theta} = 40^\circ, 45^\circ, 50^\circ, 70^\circ$, and 90°), although there may be an initial softening trend (e.g., for 40°), as we have mentioned, the laminate quickly enters a regime in which the rotation actually tends to stiffen the material, and loss of ellipticity is prevented.

As already mentioned, Fig. 4b shows that the layers rotate clockwise tending to align themselves with the principal direction of tensile deformation (*i.e.*, $\phi \to \overline{\theta} - 90^\circ$ as $\overline{\lambda} \to \infty$) for all loadings, except for the case $\overline{\theta} = 0$, for which the layers do not rotate, but instead remain coaxial with the applied deformation. Because of the apparently discontinuous behavior of the orientation angle ϕ between initial orientations of $\overline{\theta} = 0^\circ$ and 20°, and for later reference, results are also shown for intermediate (small) values of $\overline{\theta}$ in Fig. 6. Thus, the singular loading condition of pure shear at exactly $\overline{\theta} = 0$, for which the underlying layers do not rotate at all, corresponds, however, to the case for which the layers have the potential to rotate the most. To see this, it suffices to consider the infinitesimally perturbed case of pure shear at $\overline{\theta} = 0+$, for which the layers would undergo a total rotation of 90°. As will be seen in the next section, this observation will play a critical role in determining the dependence of the loss of ellipticity condition on the initial loading angle $\overline{\theta}$.

For completeness, it is noted that the effects of the evolution of the two remaining microstructural variables: the

volume fractions of the phases (18) and the repeat length (20) have proved to be of lesser importance and, for conciseness, will not be detailed here.

4.1.2. Macroscopic stability

As already discussed in the context of Fig. 4, the *overall* response of the class of Neo-Hookean laminates under investigation here can lose strong ellipticity when subjected to pure shear loading at sufficiently small angles $\overline{\theta}$ – in spite of the fact that the *local* stored-energy functions (21) and (22) are strongly elliptic (Geymonat et al., 1993). To develop this point in more detail, Fig. 7 presents results for the critical stretch, $\overline{\lambda}_{crit}$, at which Neo-Hookean laminates, with contrasts $t = 5$, 20, and 100, first lose strong ellipticity under pure shear loading conditions. Part (a) shows results for $c_0 = 30\%$ as a function of the loading angle $\overline{\theta}$. Part (b) shows results for $\overline{\theta} = 0$ as a function of the initial volume fraction c_0.

A key point to remark from Fig. 7a is that the laminates become more stable with increasing values of the loading angle $\overline{\theta}$. In fact, there is a threshold (depending on the contrast t) in $\overline{\theta}$, beyond which the response remains stable for all applied deformations. Physically, these results entail that laminates improve their macroscopic stability with decreasing amount of applied compression along the underlying layers. Indeed, under loading conditions of the form (23), $\overline{\theta} = 0$ corresponds to the case at which maximum compression is being applied along the layers. Increasing the value of $\overline{\theta}$ effectively decreases the amount of compression in the layer direction (In fact, note that for pure shear at $\overline{\theta} = 90^\circ$ the layers are essentially subjected to tension.). It is also important to recognize from Fig. 7a that increasing the contrast between the two phases, as measured by the parameter t, renders the laminate more unstable. In this regard, under loading conditions of the form (23), it can be shown that $\overline{\lambda}_{crit} \to 1$ as $t \to \infty$ for all $\overline{\theta} \neq 90^\circ$. That is, for the limiting case when the stiffer layers are taken to be rigid (i.e., for $t = \infty$), the laminate happens to be already unstable at zero strain when subjected to pure shear at an angle $\overline{\theta}$, with the exception of $\overline{\theta} = 90^\circ$. Of course, a laminate containing rigid layers is itself rigid under loading conditions that require deformation of the rigid layers, such as pure shear at an angle. The issue here is that in spite of being rigid (in the principal solution), the laminate is actually unstable when subjected to macroscopic loadings containing a compressive component of deformation along the layers.

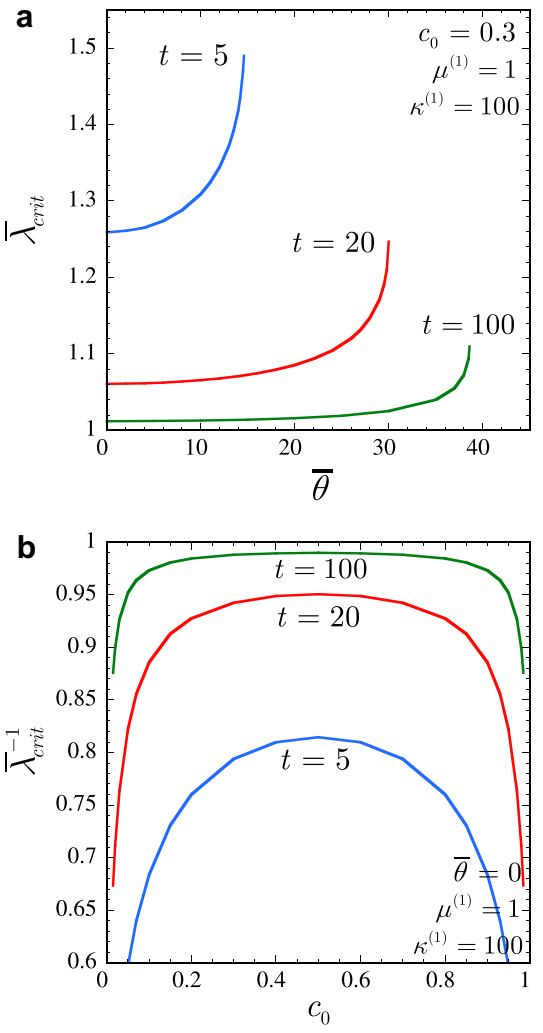

Fig. 7. The critical stretch, $\overline{\lambda}_{crit}$, at which Neo-Hookean laminates, with contrasts $t = 5, 20$, and 100, lose strong ellipticity when subjected to pure shear loading. (a) $\overline{\lambda}_{crit}$ for $c_0 = 30\%$ as a function of the loading angle $\overline{\theta}$. (b) $\overline{\lambda}_{crit}^{-1}$ for $\overline{\theta} = 0$ as a function of the initial volume fraction c_0.

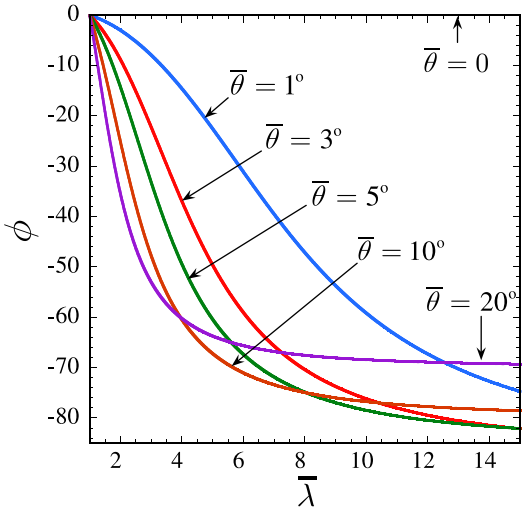

Fig. 6. Angle of rotation of the layers ϕ (given by expression (24)) in hyperelastic laminates subjected to pure shear at various small angles $\overline{\theta}$, as a function of the applied macroscopic stretch $\overline{\lambda}$. Note that the results are completely independent of the constitutive behavior of the layers.

Complementing the results shown in Fig. 7a for general $\overline{\theta}$, Fig. 7b shows that for aligned pure shear at $\overline{\theta} = 0$ – which, again, corresponds to the case of maximum compression along the layers – the laminate becomes unstable at larger stretches $\overline{\lambda}_{crit}^{-1}$ (i.e., smaller compressive strains) for higher values of the contrast t. Another interesting observation from Fig. 7b is that $\overline{\lambda}_{crit}^{-1} \to 0$ as $c_0 \to 0$. This is consistent with the fact that

phase 1 is strongly elliptic, so that in the absence of (the stiffer) phase 2 (i.e., for $c_0 = 0$) the material remains stable for all deformations. As the initial volume fraction of the stiffer layers c_0 is increased from zero, the critical stretch at which the material loses strong ellipticity $\overline{\lambda}_{crit}^{-1}$ increases monotonically up to $c_0 = 50\%$ at which $\overline{\lambda}_{crit}^{-1}$ reaches a maximum. After this point, further increase in c_0 results in the monotonic decrease of $\overline{\lambda}_{crit}^{-1}$. This behavior is simply due to the fact that phase 2 – similar to phase 1 – is strongly elliptic, so that in the limit as $c_0 \to 1$, $\overline{\lambda}_{crit}^{-1} \to 0$. In this connection, it should be mentioned that the results shown in Fig. 7b for $\overline{\lambda}_{crit}^{-1}$ are completely symmetric about $c_0 = 50\%$, the point at which the material is most unstable. Note that results similar to those shown in Fig. 7b, as well as for other types of "microscopic" instabilities, were first obtained by Triantafyllidis and Maker, 1985 for incompressible Neo-Hookean laminates.

In connection with all of the results provided in Fig. 7, it is important to remark that strong ellipticity is consistently lost here through the softening of the effective incremental shear response perpendicular to the direction of maximum applied compressive deformation. For instance, for the case of pure shear at $\overline{\theta} = 0$ presented in Fig. 7b, the laminate loses strong ellipticity because of the vanishing of $\widehat{\mathcal{L}}_{1212} = \partial^2 \widehat{W}/\partial \overline{F}_{12}^2$ at $\overline{\lambda}_{crit}$. This type of "failure" mode is consistent with the development of kink bands, which have been observed to appear in various types of stratified media (see, e.g., Kyriakides et al., 1995).

Making contact next with the earlier discussion surrounding Fig. 6, it is noticed that the more the layers can potentially rotate – that is, within the present context, the smaller the loading angle $\overline{\theta}$ – the more unstable the laminate becomes. Physically, this behavior is in accord with the idea that if the layers – and in particular, the stiff layers – rotate away from the direction of maximum applied compression, the effective incremental shear response of the laminate (in the perpendicular direction to the maximum applied compression) *softens*. It is because of this *geometric softening* that the laminate may lose strong ellipticity, even in the case when the underlying layers are made out of strongly elliptic materials.

5. Concluding remarks

In this work, we have generated explicit expressions characterizing the overall constitutive behavior and the evolution of microstructure in hyperelastic laminates subjected to finite deformations. The effect of the microstructure evolution on the effective response and macroscopic stability in these materials has been analyzed and illustrated by means of some examples.

One of the main results of this work is that the rotation of the underlying layers, which depends critically on the applied loading conditions, provides a *potential* softening mechanism for hyperelastic laminates subjected to finite strains. This mechanism depends critically on the relative orientation of the compressive loading axis to the layer direction. In particular, it has been shown that the layers rotate in such a manner that they tend to align themselves with the direction of maximum applied tensile deformation, so that the further away they are from this final destination, the more they tend to rotate, and the more important the potential softening mechanism becomes. An important consequence of the aforementioned softening mechanism is that hyperelastic laminates may lose strong ellipticity – even in the case when the materials within the underlying layers are taken to be strongly elliptic (Geymonat et al., 1993). The results indicate that the development of this type of instabilities is governed by two key "ingredients": (i) a sufficiently large compressive deformation applied along the layers, which would result in a large rotation of the layers, and (ii) a sufficiently high heterogeneity contrast between the layers.

Finally, it should be emphasized that the results presented in this paper for hyperelastic laminates are exact. In this connection, they can be useful in identifying and understanding physical mechanisms that arise in material systems with more general but related microstructures (e.g., particle-reinforced rubbers, thermoplastic elastomers) for which exact calculations are not possible. They can also be helpful in providing confidence in calculations that make use of approximate homogenization methods for more general microstructures. For example, calculations based on the application of the "second-order" homogenization method (Ponte Castañeda, 2002; Lopez-Pamies and Ponte Castañeda, 2006a) have recently unveiled analogous phenomena to those discussed in this work for the more challenging problem of fiber-reinforced elastomers (Lopez-Pamies and Ponte Castañeda, 2006b; Agoras et al., 2009).

Acknowledgements

This work was supported by Grant No. DE–FG02–04ER46110 from the Department of Energy. P.P.C. also acknowledges the support of Grant CMMI–0654063 from the National Science Foundation.

Appendix A. Overall constitutive behavior of hyperelastic laminates

In this appendix, we provide details concerning the computation – by means of the tangent second-order homogenization method (Ponte Castañeda, 1996; Ponte Castañeda and Tiberio, 2000) – of the overall constitutive behavior of the class of two-phase hyperelastic laminates studied in this work.

By making use of the general results of Ponte Castañeda and Tiberio (2000), the tangent second-order estimate for the effective stored-energy function (8) of a hyperelastic laminate, made up of two phases characterized by the stored-energy functions $W^{(1)}$ and $W^{(2)}$ with corresponding initial volume fractions $c_0^{(1)}$ and $c_0^{(2)}$, reads as:

$$\widehat{W}(\overline{\mathbf{F}}) = \sum_{r=1}^{2} c_0^{(r)} \left[W^{(r)}(\overline{\mathbf{F}}^{(r)}) + \frac{1}{2} \mathcal{S}^{(r)}(\overline{\mathbf{F}}^{(r)}) \cdot (\overline{\mathbf{F}} - \overline{\mathbf{F}}^{(r)}) \right]. \tag{25}$$

In this expression, it is recalled that $\boldsymbol{\mathcal{S}}^{(r)}(\overline{\mathbf{F}}^{(r)}) = \partial W^{(r)}(\overline{\mathbf{F}}^{(r)})/\partial \mathbf{F}$ and $\overline{\mathbf{F}}^{(r)}$ denotes the average deformation gradient of phase r in a *linear comparison composite* (LCC) with the *same microstructure* – in the undeformed configuration – as the original hyperelastic composite and with *local* stored-energy functions given by:

$$W_T^{(r)}(\mathbf{F}) = W^{(r)}(\overline{\mathbf{F}}^{(r)}) + \boldsymbol{\mathcal{S}}^{(r)}(\overline{\mathbf{F}}^{(r)}) \cdot (\mathbf{F} - \overline{\mathbf{F}}^{(r)}) + \frac{1}{2}(\mathbf{F} - \overline{\mathbf{F}}^{(r)}) \cdot \boldsymbol{\mathcal{L}}^{(r)}(\overline{\mathbf{F}}^{(r)})(\mathbf{F} - \overline{\mathbf{F}}^{(r)}), \tag{26}$$

where it is recalled that $\boldsymbol{\mathcal{L}}^{(r)}(\overline{\mathbf{F}}^{(r)}) = \partial^2 W^{(r)}(\overline{\mathbf{F}}^{(r)})/\partial \mathbf{F}^2$.

The *overall* stored-energy function $\widehat{W}_T$ for the above-defined LCC may be expressed (see, e.g., Lopez-Pamies and Ponte Castañeda, 2006b) as follows:

$$\widehat{W}_T(\overline{\mathbf{F}}) = \widetilde{g} + \widetilde{\mathbf{T}} \cdot \overline{\mathbf{F}} + \frac{1}{2}\overline{\mathbf{F}} \cdot \widetilde{\mathbf{L}}\overline{\mathbf{F}}, \tag{27}$$

where $\widetilde{g} = \overline{g} + \frac{1}{2}(\triangle\boldsymbol{\mathcal{L}})^{-1}\triangle\mathbf{T} \cdot (\widetilde{\mathbf{L}} - \overline{\boldsymbol{\mathcal{L}}})(\triangle\boldsymbol{\mathcal{L}})^{-1}\triangle\mathbf{T}$, $\widetilde{\mathbf{T}} = \overline{\mathbf{T}} + (\widetilde{\mathbf{L}} - \overline{\boldsymbol{\mathcal{L}}})(\triangle\boldsymbol{\mathcal{L}})^{-1}\triangle\mathbf{T}$ are *effective* quantities depending on $\widetilde{\mathbf{L}}$, which stands for the effective modulus tensor of the LCC. For the class of laminates of interest in this work, the exact $\widetilde{\mathbf{L}}$ is known to be given by the Hashin–Shtrikman relation (see, e.g., Chapter 9 in Milton, 2002):

$$\widetilde{\mathbf{L}} = \boldsymbol{\mathcal{L}}^{(1)}(\overline{\mathbf{F}}^{(1)}) + c_0^{(2)}\left[c_0^{(1)}\mathbf{H} - \Delta\boldsymbol{\mathcal{L}}^{-1}\right]^{-1}, \tag{28}$$

where $\triangle\boldsymbol{\mathcal{L}} = \boldsymbol{\mathcal{L}}^{(1)}(\overline{\mathbf{F}}^{(1)}) - \boldsymbol{\mathcal{L}}^{(2)}(\overline{\mathbf{F}}^{(2)})$ and the microstructural tensor $\mathbf{H}$ is given by expression (17) in the main body of the text. Also, in the above expressions, $g^{(r)} = W^{(r)}(\overline{\mathbf{F}}^{(r)}) - \mathbf{T}^{(r)} \cdot \overline{\mathbf{F}}^{(r)} - \frac{1}{2}\overline{\mathbf{F}}^{(r)} \cdot \boldsymbol{\mathcal{L}}^{(r)}(\overline{\mathbf{F}}^{(r)})\overline{\mathbf{F}}^{(r)}$, $\mathbf{T}^{(r)} = \boldsymbol{\mathcal{S}}^{(r)}(\overline{\mathbf{F}}^{(r)}) - \boldsymbol{\mathcal{L}}^{(r)}(\overline{\mathbf{F}}^{(r)})\overline{\mathbf{F}}^{(r)}$, and $\triangle\mathbf{T} = \mathbf{T}^{(1)} - \mathbf{T}^{(2)}$. Furthermore, $\overline{g} = c_0^{(1)}g^{(1)} + c_0^{(2)}g^{(2)}$, $\overline{\mathbf{T}} = c_0^{(1)}\mathbf{T}^{(1)} + c_0^{(2)}\mathbf{T}^{(2)}$, and $\overline{\boldsymbol{\mathcal{L}}} = c_0^{(1)}\boldsymbol{\mathcal{L}}^{(1)}(\overline{\mathbf{F}}^{(1)}) + c_0^{(2)}\boldsymbol{\mathcal{L}}^{(2)}(\overline{\mathbf{F}}^{(2)})$.

The average deformation gradients $\overline{\mathbf{F}}^{(1)}$ and $\overline{\mathbf{F}}^{(2)}$ – needed in the computation of the tangent second-order estimate (25) – can be expediently computed from knowledge of the effective stored-energy function (27) (see, e.g., Lopez-Pamies and Ponte Castañeda, 2006a for a derivation). The final expressions may be cast as

$$\overline{\mathbf{F}} - \overline{\mathbf{F}}^{(1)} = \mathbf{H}\left[\boldsymbol{\mathcal{L}}^{(1)}(\overline{\mathbf{F}}^{(1)})(\overline{\mathbf{F}} - \overline{\mathbf{F}}^{(1)}) + c_0^{(2)}\Delta\boldsymbol{\mathcal{S}}\right] \tag{29}$$

with $\Delta\boldsymbol{\mathcal{S}} = \boldsymbol{\mathcal{S}}^{(1)}(\overline{\mathbf{F}}^{(1)}) - \boldsymbol{\mathcal{S}}^{(2)}(\overline{\mathbf{F}}^{(2)})$ and

$$\overline{\mathbf{F}}^{(2)} = \frac{1}{c_0^{(2)}}\overline{\mathbf{F}} - \frac{c_0^{(1)}}{c_0^{(2)}}\overline{\mathbf{F}}^{(1)}. \tag{30}$$

In connection with the above relations, it is useful to note that (30) provides an *explicit* expression for $\overline{\mathbf{F}}^{(2)}$ in terms of $\overline{\mathbf{F}}$ and $\overline{\mathbf{F}}^{(1)}$. This allows relation (29) to be considered as an *implicit* tensorial equation for $\overline{\mathbf{F}}^{(1)}$. In this regard, it is convenient to simplify further Eq. (29) by making use of the specific form (17). The result reads as follows:

$$\overline{F}_{ij} - \overline{F}_{ij}^{(1)} = K_{ik}^{-1}N_lN_j\left[\mathcal{L}_{klpq}^{(1)}(\overline{\mathbf{F}}^{(1)})(\overline{F}_{pq} - \overline{F}_{pq}^{(1)}) + c_0^{(2)}(\mathcal{S}_{kl}^{(1)}(\overline{\mathbf{F}}^{(1)}) - \mathcal{S}_{kl}^{(2)}(\overline{\mathbf{F}}^{(2)}))\right], \tag{31}$$

where it is recalled that $K_{ik} = \mathcal{L}_{ijkl}^{(1)}(\overline{\mathbf{F}}^{(1)})N_jN_l$. Now, it is straightforward to realize that multiplying Eq. (31) with $N_j^{\perp 2}$ and $N_j^{\perp 3}$ leads to equations (12) of Section 3. For continuity, we repeat these equations here:

$$[\overline{\mathbf{F}} - \overline{\mathbf{F}}^{(1)}]\mathbf{N}^{\perp 2} = \mathbf{0} \quad \text{and} [\overline{\mathbf{F}} - \overline{\mathbf{F}}^{(1)}]\mathbf{N}^{\perp 3} = \mathbf{0}. \tag{32}$$

Note that relations (32) constitute a system of 6 *linear* equations for 6 components of $\overline{\mathbf{F}}^{(1)}$. The closed-form solution to this system renders

$$\overline{\mathbf{F}}^{(1)} = \overline{\mathbf{F}} + \mathbf{a} \otimes \mathbf{N}, \tag{33}$$

which corresponds to relation (14) in the main body of the text. In this last relation, $\mathbf{a}$ denotes an arbitrary vector (with 3 unknown components). The remaining 3 components needed to completely specify $\overline{\mathbf{F}}^{(1)}$ must be determined from the 3 remaining scalar equations in (31). To this end, use is made of (33) in (31) and the result multiplied with N_j. The resulting equation reads as follows:

$$a_i = K_{ik}^{-1}\left[\mathcal{L}_{klpq}^{(1)}(\overline{\mathbf{F}}^{(1)})N_lN_qa_p - c_0^{(2)}(\mathcal{S}_{kl}^{(1)}(\overline{\mathbf{F}}^{(1)}) - \mathcal{S}_{kl}^{(2)}(\overline{\mathbf{F}}^{(2)}))N_l\right]. \tag{34}$$

Next, by left-multiplying (34) with $\mathbf{K}$, the following equation is obtained:

$$K_{ij}a_j = \mathcal{L}_{imjn}^{(1)}(\overline{\mathbf{F}}^{(1)})N_mN_na_j = \mathcal{L}_{ilpq}^{(1)}(\overline{\mathbf{F}}^{(1)})N_lN_qa_p - c_0^{(2)}(\mathcal{S}_{il}^{(1)}(\overline{\mathbf{F}}^{(1)}) - \mathcal{S}_{il}^{(2)}(\overline{\mathbf{F}}^{(2)}))N_l, \tag{35}$$

which after a trivial simplification can be finally rewritten as Eq. (13) of Section 3. Again, for convenience, we repeat such equation here:

$$[\boldsymbol{\mathcal{S}}^{(1)}(\overline{\mathbf{F}}^{(1)}) - \boldsymbol{\mathcal{S}}^{(2)}(\overline{\mathbf{F}}^{(2)})]\mathbf{N} = \mathbf{0}. \tag{36}$$

In summary, 6 out of the 9 scalar equations contained in (29) have been recast as a system of 6 *linear* equations, given by relations (32). These linear equations can be solved in closed form for 6 components of $\overline{\mathbf{F}}^{(1)}$. The remaining 3 equations in (29), which have been conveniently rewritten as (36), constitute a *closed* system of 3 *nonlinear* equations for the remaining 3 components of $\overline{\mathbf{F}}^{(1)}$. In general, these 3 equations must be solved numerically. Having computed the values of all the components of $\overline{\mathbf{F}}^{(1)}$ for a given $\overline{\mathbf{F}}$, the values of the components of $\overline{\mathbf{F}}^{(2)}$ can be readily determined using the global average condition (30). In turn, the tangent second-order estimate for the effective stored-energy function $\widehat{W}$ of hyperelastic laminates can then be computed, from expression (25), using these results. In this connection, it is important to recognize that the stored-energy function (25) simplifies eventually to relation (10) given in the text. This is easy to see from the fact that $\overline{\mathbf{F}}^{(1)}$—as well as $\overline{\mathbf{F}}^{(2)}$—is of the form (33) and the stress quantities $\boldsymbol{\mathcal{S}}^{(1)}$ and $\boldsymbol{\mathcal{S}}^{(2)}$ must satisfy the jump condition (36).

Next, the effective stress associated with the stored-energy function (10) is given by

$$\overline{\mathbf{S}} = \frac{\partial\widehat{W}}{\partial\overline{\mathbf{F}}}(\overline{\mathbf{F}}) = c_0^{(1)}\boldsymbol{\mathcal{S}}^{(1)}(\overline{\mathbf{F}}^{(1)})\frac{\partial\overline{\mathbf{F}}^{(1)}}{\partial\overline{\mathbf{F}}} + c_0^{(2)}\boldsymbol{\mathcal{S}}^{(2)}(\overline{\mathbf{F}}^{(2)})\frac{\partial\overline{\mathbf{F}}^{(2)}}{\partial\overline{\mathbf{F}}}, \tag{37}$$

which, upon use of the average condition (30) once again, may be rewritten as follows:

$$\overline{\mathbf{S}} = c_0^{(1)}\Delta\boldsymbol{\mathcal{S}}\frac{\partial\overline{\mathbf{F}}^{(1)}}{\partial\overline{\mathbf{F}}} + \boldsymbol{\mathcal{S}}^{(2)}(\overline{\mathbf{F}}^{(2)}). \tag{38}$$

Expression (38) can be simplified further by recognizing from (33) that the partial derivative of $\overline{\mathbf{F}}^{(1)}$ with respect to $\overline{\mathbf{F}}$ is of the form

$$\frac{\partial \overline{F}^{(1)}_{ij}}{\partial \overline{F}_{kl}} = \delta_{ik}\delta_{jl} + \frac{\partial a_i}{\partial \overline{F}_{kl}} N_j, \tag{39}$$

where δ_{ij} is the Kronecker delta. It then follows immediately from (39) and (36) that the macroscopic stress can be ultimately simplified to expression (15) of Section 3.

Similarly, the effective incremental modulus tensor associated with the estimate (10) can be computed by taking the partial derivative of $\overline{\mathbf{S}}$ in (15) with respect to the macroscopic deformation gradient $\overline{\mathbf{F}}$. Making use of (30), the effective incremental modulus tensor can be written as

$$\widehat{\mathcal{L}} = \frac{\partial^2 \widehat{W}}{\partial \overline{\mathbf{F}} \partial \overline{\mathbf{F}}}(\overline{\mathbf{F}}) = c_0^{(1)} \Delta \mathcal{L} \frac{\partial \overline{\mathbf{F}}^{(1)}}{\partial \overline{\mathbf{F}}} + \mathcal{L}^{(2)}(\overline{\mathbf{F}}^{(2)}). \tag{40}$$

At this stage, it is interesting to notice the parallel between expression (40) for the effective incremental modulus $\widehat{\mathcal{L}}$, and expression (38) for the macroscopic stress $\overline{\mathbf{S}}$. Note, however, that in contrast to (38) – which could be ultimately rewritten as (15) by making use of the form of $\partial \overline{\mathbf{F}}^{(1)}/\partial \overline{\mathbf{F}}$ given by (39) – expression (40) requires precise knowledge of the dependence – not only of the form (39) – of $\partial \overline{\mathbf{F}}^{(1)}/\partial \overline{\mathbf{F}}$ on $\overline{\mathbf{F}}^{(1)}$ in order to be simplified further. This is simply because the difference $(\mathcal{L}^{(1)} - \mathcal{L}^{(2)})$ – as opposed to $(\mathcal{S}^{(1)} - \mathcal{S}^{(2)})$ – need *not* satisfy any jump conditions. In this connection, with the aim of generating an explicit expression for $\partial \overline{\mathbf{F}}^{(1)}/\partial \overline{\mathbf{F}}$ in terms of $\overline{\mathbf{F}}^{(1)}$, we first take the partial derivative of Eqs. (32 and 36) with respect to $\overline{\mathbf{F}}$. The resulting equations can be conveniently written as follows:

$$\frac{\partial \overline{F}^{(1)}_{ij}}{\partial \overline{F}_{kl}} N_j^{\perp 2} = \delta_{ik}\delta_{jl} N_j^{\perp 2}, \quad \frac{\partial \overline{F}^{(1)}_{ij}}{\partial \overline{F}_{kl}} N_j^{\perp 3} = \delta_{ik}\delta_{jl} N_j^{\perp 3}, \quad (c_0^{(2)} \mathcal{L}^{(1)}_{ijkl}(\overline{\mathbf{F}}^{(1)}) - c_0^{(1)} \mathcal{L}^{(2)}_{ijkl}(\overline{\mathbf{F}}^{(2)})) \frac{\partial \overline{F}^{(1)}_{kl}}{\partial \overline{F}_{mn}} N_j = \mathcal{L}^{(2)}_{ijmn} N_j. \tag{41}$$

Now, it is noted that relations (41) constitute a system of 81 *linear* equations for the 81 components of the fourth-order tensor $\partial \overline{\mathbf{F}}^{(1)}/\partial \overline{\mathbf{F}}$. Finally, upon solving these equations, the following *explicit* expression for $\partial \overline{\mathbf{F}}^{(1)}/\partial \overline{\mathbf{F}}$ in terms of $\overline{\mathbf{F}}^{(1)}$ is obtained:

$$\frac{\partial \overline{\mathbf{F}}^{(1)}}{\partial \overline{\mathbf{F}}} = \frac{1}{c_0^{(1)}} \mathcal{I} + \frac{c_0^{(2)}}{c_0^{(1)}} [c_0^{(1)} \mathbf{H} \Delta \mathcal{L} - \mathcal{I}]^{-1}, \tag{42}$$

where $\mathcal{I}$ denotes the identity operator in the space of fourth-order tensors (i.e., $\mathcal{I}_{ijkl} = \delta_{ik}\delta_{jl}$), and it is recalled that $\mathbf{H}$ is given by expression (17). Having determined $\partial \overline{\mathbf{F}}^{(1)}/\partial \overline{\mathbf{F}}$, it is now straightforward to show that the effective incremental modulus (40) may be finally rewritten as expression (16) of Section 3.

As a final remark, it is interesting to notice here that relation (16) coincides identically with the Hashin–Shtrikman expression (28) for the effective modulus tensor of the relevant LCC. The effective incremental modulus associated with the tangent second-order estimate is not equal, in general, to the effective modulus of the auxiliary LCC (i.e., $\widehat{\mathcal{L}} \neq \widetilde{\mathbf{L}}$). However, for the special case of laminate microstructures, the *linear* comparison composite, defined by (26)–(28), is *exactly equivalent* to the *nonlinear* composite and thus, $\widehat{\mathcal{L}} = \widetilde{\mathbf{L}}$.

Appendix B. Evolution of microstructural variables in hyperelastic laminates

In this appendix, we sketch out the derivations of the expressions presented in Section 3.2 for the evolution of volume fractions, direction of lamination, and repeat length in hyperelatic laminates subjected to finite deformations.

First, the current volume fractions of the phases in the deformed configuration, as given by expressions (18) in the main body of the text, can be simply determined as follows:

$$c^{(r)} \doteq \frac{\int_{\Omega^{(r)}} \mathrm{d}v}{\int_{\Omega} \mathrm{d}v} = \frac{\int_{\Omega_0^{(r)}} \det \mathbf{F} \mathrm{d}V}{\int_{\Omega_0} \det \mathbf{F} \mathrm{d}V} = \frac{\det \overline{\mathbf{F}}^{(r)}}{\det \overline{\mathbf{F}}} c_0^{(r)}. \tag{43}$$

Here, Ω and $\Omega^{(r)}$ denote the volumes of the specimen and phase r in the *deformed* configuration, respectively, and critical use has been made of the fact that $\det \mathbf{F}$ is a null-Lagrangian, as well as that the deformation gradient field is constant per phase.

Next, by virtue of Nanson's formula – together with the facts that layer interfaces are material surfaces and the deformation gradient field is constant per phase – it follows that the current direction of lamination in the deformed configuration is given by:

$$\mathbf{n} = \|\overline{\mathbf{F}}^{(1)-T}\mathbf{N}\|^{-1} \overline{\mathbf{F}}^{(1)-T}\mathbf{N} \tag{44}$$

or

$$\mathbf{n} = \|\overline{\mathbf{F}}^{(2)-T}\mathbf{N}\|^{-1} \overline{\mathbf{F}}^{(2)-T}\mathbf{N}. \tag{45}$$

Making use now of expression (14) for $\overline{\mathbf{F}}^{(1)}$, it is not difficult to show that

$$\overline{\mathbf{F}}^{(1)-T} = \overline{\mathbf{F}}^{-T} - \frac{1}{1 + \overline{\mathbf{F}}^{-1}\mathbf{a} \cdot \mathbf{N}} \overline{\mathbf{F}}^{-T}\mathbf{N} \otimes \overline{\mathbf{F}}^{-1}\mathbf{a}, \tag{46}$$

and hence, that (44) may be ultimately simplified to

$$\mathbf{n} = \|\overline{\mathbf{F}}^{-T}\mathbf{N}\|^{-1} \overline{\mathbf{F}}^{-T}\mathbf{N}, \tag{47}$$

as given by expression (19) in the main body of the text. Of course, expression (45) can also be shown to reduce identically to relation (47). This can be readily accomplished by first recognizing that (similar to the form (14) for $\overline{\mathbf{F}}^{(1)})\overline{\mathbf{F}}^{(2)} = \overline{\mathbf{F}} - c_0^{(1)}/c_0^{(2)} \mathbf{a} \otimes \mathbf{N}$, appropriately adapting (46) to generate an explicit expression for $\overline{\mathbf{F}}^{(2)-T}$, and then utilizing this result to simplify (45).

Finally, attention is turned to the derivation of expression (20) for the current repeat length of the laminate in the deformed configuration. To this end, first it is helpful to define a *unit cell* (or periodically repeating building block) for the laminate. For convenience, we take here two entire adjacent layers as the unit cell (see Fig. 8a). Within this context it is then expedient to realize that the initial repeat length in the undeformed configuration may be expressed as follows:

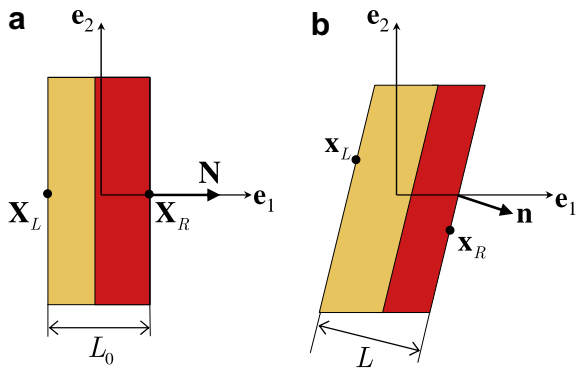

Fig. 8. (a) Schematic representation of a unit cell made up of two adjacent layers in the undeformed configuration. In this figure, $\mathbf{N}$ and L_0 denote, respectively, the initial direction of lamination and repeat length of the laminate. Moreover, $\mathbf{X}_L$ and $\mathbf{X}_R$ denote arbitrary material points on the left and right boundary of the unit cell. (b) The same unit cell in the deformed configuration.

$$L_0 = \frac{\|\mathbf{N}\cdot(\mathbf{X}_R - \mathbf{X}_L)\|}{\|\mathbf{N}\|} = \|\mathbf{N}\cdot(\mathbf{X}_R - \mathbf{X}_L)\|, \tag{48}$$

where it is recalled that the unit vector $\mathbf{N}$ stands for the initial direction of lamination. Moreover, $\mathbf{X}_L$ denotes an arbitrary material point in the far left boundary – characterized by the plane equation $\mathbf{N}\cdot(\mathbf{X}-\mathbf{X}_L)=0$ – of the unit cell, as depicted by Fig. 8a. Similarly, $\mathbf{X}_R$ denotes an arbitrary material point in the far right boundary – characterized by the plane equation $\mathbf{N}\cdot(\mathbf{X}-\mathbf{X}_R)=0$ – of the unit cell (see Fig. 8(*a*)). Making use of the results stated in the preceding paragraph, it then follows that the left and right boundaries of the unit cell in the undeformed configuration (i.e., the planes $\mathbf{N}\cdot(\mathbf{X}-\mathbf{X}_L)=0$ and $\mathbf{N}\cdot(\mathbf{X}-\mathbf{X}_R)=0$) evolve, respectively, to the planes $\mathbf{n}\cdot(\mathbf{x}-\mathbf{x}_L)=0$ and $\mathbf{n}\cdot(\mathbf{x}-\mathbf{x}_R)=0$ in the *deformed* configuration. In these expressions, $\mathbf{n}$ is given by (47) and $\mathbf{x}_L = \overline{\mathbf{F}}\mathbf{X}_L$ and $\mathbf{x}_R = \overline{\mathbf{F}}\mathbf{X}_R$ are the current positions of the material points $\mathbf{X}_L$ and $\mathbf{X}_R$ in the deformed configuration, as schematically illustrated by Fig. 8b. Having established these results, it is then straightforward to conclude that the initial repeat length (48) evolves to:

$$L = \frac{\|\mathbf{n}\cdot(\mathbf{x}_R - \mathbf{x}_L)\|}{\|\mathbf{n}\|} = \|\overline{\mathbf{F}}^{-T}\mathbf{N}\|^{-1}L_0 \tag{49}$$

in the deformed configuration, as given by expression (20) in the main body of the text.

References

Agoras, M., Lopez-Pamies, O., Ponte Castañeda, P., 2009. A general hyperelastic model for incompressible fiber-reinforced elastomers. J. Mech. Phys. Solids 57, 268–286.

Cohen, Y., Albalak, R.J., Dair, B.J., Capel, M.S., Thomas, E.L., 2000. Deformation of oriented lamellar block copolymer films. Macromolecules 33, 6502–6516.

Geymonat, G., Müller, S., Triantafyllidis, N., 1993. Homogenization of nonlinearly elastic materials, microscopic bifurcation and macroscopic loss of rank-one convexity. Arch. Rat. Mech. Analysis 122, 231–290.

Hill, R., 1972. On constitutive macro-variables for heterogeneous solids at finite strain. Proc. R. Soc. Lond. A 326, 131–147.

Kyriakides, S., Arseculeratne, R., Perry, E.J., Liechti, K.M., 1995. On the compressive failure of fiber reinforced composites. Int. J. Solids Structures 32, 689–738.

Lopez-Pamies, O., 2006. On the effective behavior, microstructure evolution, and macroscopic stability of elastomeric composites. Ph.D. Dissertation, University of Pennsylvania, USA..

Lopez-Pamies, O., Ponte Castañeda, P., 2006a. On the overall behavior, microstructure evolution, and macroscopic stability in reinforced rubbers at large deformations. I – Theory. J. Mech. Phys. Solids 54, 807–830.

Lopez-Pamies, O., Ponte Castañeda, P., 2006b. On the overall behavior, microstructure evolution, and macroscopic stability in reinforced rubbers at large deformations II – application to cylindrical fibers. J. Mech. Phys. Solids 54, 831–863.

Milton, G.W., 2002. The theory of composites. Cambridge Monographs on Applied and Computational Mathematics, vol. 6. Cambridge University Press, Cambridge.

Nestorvic, N., Triantafyllidis, N., 2004. Onset of failure in finitely strained layered composites subjected to combined normal and shear strain. J. Mech. Phys. Solids 52, 941–974.

Ponte Castañeda, P., 1996. Exact second-order estimates for the effective mechanical properties of nonlinear composite materials. J. Mech. Phys. Solids 44, 827–862.

Ponte Castañeda, P., 2002. Second-order homogenization estimates for nonlinear composites incorporating field fluctuations I. Theory. J. Mech. Phys. Solids 50, 737–757.

Ponte Castañeda, P., Tiberio, E., 2000. A second-order homogenization method in finite elasticity and applications to black-filled elastomers. J. Mech. Phys. Solids 48, 1389–1411.

Triantafyllidis, N., Maker, B.N., 1985. On the comparison between microscopic and macroscopic instability mechanisms in a class of fiber-reinforced composites. J. Appl. Mech. 52, 794–800.

Triantafyllidis, N., Nestorvić, M.D., Schraad, M.W., 2006. Failure surfaces for finitely strained two-phase periodic solids under general in-plane loading. J. Appl. Mech. 73, 505–515.